An application of the artificial neural network to optimise the energy performances of a magnetic refrigerator

Ciro Aprea[a,1], Adriana Greco[b], Angelo Maiorino[a,2,*]

[a] *Department of Industrial Engineering, University of Salerno, Via Giovanni Paolo II 132, 84084, Fisciano (SA), Italy*
[b] *Department of Industrial Engineering, University of Naples Federico II, P.le Tecchio 80, 80125, Napoli, Italy*

Abstract

This paper treats a control technique designed to maximise the working of a rotary permanent magnets magnetic refrigerator (RPMMR). The method, named ANNTEO, is based on the use of the artificial neural networks (ANNs), which have demonstrated to predict well the energy performances of an actual RPMMR obtaining a good agreement with the experimental tests. The ANN gives the possibility to carry out a working map, and then, applying an optimisation process, it is possible to catch the optimal working point regarding the number of revolution of the magnets per minute and the volumetric flow rate of the regenerating fluid. In particular, the optimisation can be processed with the aim to maximise the COP (energy saving) or the cooling capacity (time-saving). As a proof of the concept, this paper reports an example of an application of the ANNTEO. Also, new perspectives on the use of the ANNs in the magnetic refrigeration field are proposed.

Keywords: magnetic refrigeration; artificial neural network; magnetocaloric effect; numerical model; controller; optimization

---

* *Corresponding author: Tel. +39 (0) 89 964002; fax +39 089 964037;*
E-mail: amaiorino@unisa.it (A. Maiorino).
[1] *Member of IIR-IIF Commission E2.*
[2] *Member of IIR-IIF.*

Nomenclature

Acronyms

AMR	active magnetic regenerator
ANN	artificial neural network
ANNTEO	Artificial Neural Network Technique for Energy Optimisation
BP	error back propagation algorithm
COP	coefficient of performance
MCM	magnetocaloric material
MLP	multi-layer perceptron
MSE	mean square error
RPMMR	rotary permanent magnets magnetic refrigerator
vv	various or generic unit of measurements concerning the dimension at which the symbol is referred

Symbols

$\mathbf{b_1}$	vector of the biases at the hidden layer	[-]
$\mathbf{b_2}$	vector of the biases at the output layer	[-]
c_f	specific heat of the regenerating fluid	[JkgK^{-1}]
c_{MCM}	specific heat of the magnetocaloric material (here gadolinium)	[JkgK^{-1}]
$\overline{COP}$	matrix of the COP predicted by the ANN	[-]
$\mathbb{D}_{in}$	domain of the input in $\mathbb{R}^4$ as defined in Eq. 12	[-]
γ	transfer function in the output layer	[-]
ΔT_{req}	required ΔT_{SET}	[K]
ΔT_{SET}	temperature span at ends of the device and due to actual conditions (see Eq. 6)	[K]
$\mathbf{\Delta T_{SET}}$	array of ΔT_{SET}	[K]
ΔT_{span}	temperature span at ends of the device	[K]
ΔT^p	p-element of the $\mathbf{\Delta T_{SET}}$ array	[K]
ΔT_{CHX}	difference between the $T_{SET,POIN}$ and the temperature at the hot end of the refrigerator	[K]
ΔT_{HHX}	difference between the T_H and the temperature at the hot end of the refrigerator	[K]
δ	absolute error	[-]
ε_{COP}	relative error for the COP	[%]

$\varepsilon_{\dot{Q}_{ref}}$	relative error for the $\dot{Q}_{ref}$	[%]
f_{AMR}	cycle frequency	[Hz]
φ	transfer function in the hidden layer	[-]
θ_f	rotation angle for which the fluid is stopped	[rad]
θ_i	rotation angle for which the fluid start to blow through the regenerator	[rad]
Input	matrix of the inputs of the ANN	[vv]
$\mathbf{input_{hj}}$	array (1x4) representing the hj-element of the Input matrix	[vv]
$\bar{I}_W$	matrix of the weights of the hidden neurones	[-]
$\bar{L}_W$	matrix of the weights of the output neurones	[-]
M_f	mass of the regenerating fluid	[kg]
M_{MCM}	mass of the magnetocaloric material	[kg]
n_{rpm}	rotation of the magnets per minutes	[rpm]
$\mathbf{n_{rpm}}$	array (1xk) of the rotations of the magnets per minutes	[rpm]
$n_{rpm,h}$	h-element of $\mathbf{n}_{rpm}$ array	[rpm]
N_{hn}	number of hidden neurones	[-]
N_i	number of the input neurones	[-]
P_{in}	pressure at the inlet of the pump	[Pa]
P_{out}	pressure at the outlet of the pump	[Pa]
ρ_f	density of the regenerating fluid	[k gm^{-3}]
R^2	absolute fraction of variation	[-]
$\dot{Q}_{ref}$	cooling capacity, refrigeration power	[W]
$\overline{\dot{Q}_{ref}}$	matrix of the $\dot{Q}_{ref}$ predicted by the ANN	[W]
$\dot{Q}_{req}$	required $\dot{Q}_{ref}$	[W]
T	array of T_H	[K]
T_H	temperature of heat rejection	[K]
$T_{H,req}$	required T_H	[K]
T_{HFi}	temperature of the regenerating fluid entering the hot side of the refrigerator	[K]
T_{HFo}	temperature of the regenerating fluid outgoing from the hot side of the refrigerator	[K]
T_{LFo}	temperature of the regenerating fluid outgoing from the cold side of the refrigerator	[K]
T^q	q-element of the $\mathbf{T_H}$ array	[K]
$T_{SET,point}$	Temperature level of the air inner to the refrigerator required by the user	[K]
UF	utilisation factor	[-]

$\dot{V}_f$	volumetric flow rate of the regenerating fluid	[l min^{-1}]
$\dot{\mathbf{V}}_\mathbf{f}$	array (1xh) of the volumetric flow rates of the regenerating fluid	[l min^{-1}]
$\dot{V}_{f,j}$	j-element of the $\dot{\mathbf{V}}_\mathbf{f}$ array	[l min^{-1}]
w_i	ith synaptic weight	[-]
$\dot{W}_{el,h}$	electrical power absorbed by the electric heater	[W]
$\dot{W}_p$	electrical power absorbed by the pump	[W]
$\overline{\dot{W}_p}$	matrix of the $\dot{W}_p$ predicted by the ANN	[W]
$\dot{W}_m$	electrical power absorbed by the electric motor	[W]
$\overline{\dot{W}_m}$	matrix of the $\dot{W}_m$ predicted by the ANN	[W]
Y	vector representing the ANN for the kjth input	[vv]
$\bar{Y}$	matrix representing the ANN	[vv]
$\mathbf{Y}$	vector function representing the ANN in $\mathbb{R}^4$	[vv]
$\mathbf{Y_{con}}$	vector function representing the ANN in $\mathbb{R}^4$ under the operational constraints	[vv]
Y(x)	ANN approximation	[vv]
y(x)	actual value	[vv]
$^{\langle \Delta T^p, T^q \rangle}$	for a generic couple of values of ΔT_{SET} and T_H	[-]
x	input	[vv]
$\mathbf{x}$	array of the inputs	[vv]

1. Introduction

Over the last decade, magnetic refrigeration at room temperature has attracted a growing number of researchers, which has helped to expand our knowledge significantly. Although the primary objective of creating the first magnetic refrigerator for commercial use at ambient temperatures has not yet been realised, optimism has begun to leak through. In fact, several companies have begun to show some interest in this field in recent years, and various international funds have been allocated for research and industry partnerships. However, as evidenced by Didier Coulomb in the aftermath of the VII Conference on Magnetic Refrigeration, researchers must focus their attention on finding cheaper magnetocaloric materials, as well as on the improvement of these systems by introducing new architectures and optimising the operation of the existing frameworks (Coulomb, 2016). As part of the implementation of new designs, observing the most current review (Kitanovski et al., 2015) and the newest concepts presented in the last two years (Lozano et al., 2016; Trevizoli et al., 2016; Velázquez et al., 2016), the rotary permanent magnet magnetic refrigerator (RPMMR) seem to serve as the reference standard, with variations in the number of magnetic poles and the number of regenerators. As proof of this, the optimisation problem has played a larger role in recent times. Some researchers have focused their attention on the aspects related to the optimisation of regenerators (Bahl et al., 2017; Benedict et al., 2017a; Lei et al., 2015; Roy et al., 2017; Tušek et al., 2013a); others have taken into account the possibility of optimising the distribution of regenerating fluid through the regenerators (Eriksen et al., 2016; Teyber et al., 2016; Trevizoli et al., 2014); while others have analysed a better use of magnetic refrigeration, coupling it to renewable energy sources (Aprea et al., 2015). In addition, some researchers have considered other theoretical aspects, such as cost optimisation (Bjørk et al., 2016, 2011; Tura and Rowe, 2014), the life cycle assessment (Monfared et al., 2014), the optimisation multi-objective (Bouchekara et al., 2014) and the incidence of the properties of magnetocaloric materials on the optimisation of the design (Benedict et al., 2017b). However, the optimisation problem is not to be considered only in the design and realization of a refrigerator, but be given the level of maturity of the magnetic refrigeration and the ever closer commercialization of magnetic refrigerators (Coulomb, 2016); ; it is appropriate that the world of research begins to wonder about the possibility of optimising the operation of a machine as it is. In this sense, it is necessary to identify a methodology that can instruct a control system, which can manage a magnetic refrigerator in various operating conditions with the aim to improve the energy performances. Although, from the user's side, a magnetic refrigerator is identical to a classic refrigerator (characterised by a demand and a supply of cooling energy at fixed temperature levels),

from the operational side it has an entirely different behaviour. In the past, various authors (Bahl et al., 2014; Lozano et al., 2014; Tura and Rowe, 2011; Tušek et al., 2013b; Zimm et al., 2007) have investigated the operating dynamics of magnetic refrigerators, highlighting two fundamental aspects: non-linear behaviour and dependence on performance of various parameters simultaneously. To address the lack of works, which focus on the issue of the control, in this paper, a control technique designed to optimise the functioning of an RPMMR is introduced. The method presents a further innovation in the field of magnetic refrigeration: the use of neural networks. For the first time, RPMMR is discussed regarding their applicability, and their uses will subsequently be described for optimisation of the operation.

2. The Artificial Neural Networks

An ANN is a mathematical tool based on the functioning of the human brain and is utilised for a large variety of tasks (such as classification, data mining, pattern recognition, image compression, and process modelling). The main advantages of the ANN, compared to other expert systems, are its speed, simplicity, and ability to model a multivariable problem to solve complex relationships between the input and output of the variables. This method provides the nonlinear relationships between input and output parameters employing a training data. Therefore, the ANN method overcomes the limitations of conventional approaches by extracting the required information and predicting the desired output of the system using experimental data, without requiring any particular analytical equations (Mohanraj et al., 2011). The ANN essential components are the perceptron which emulates the behaviour of the human neurones.

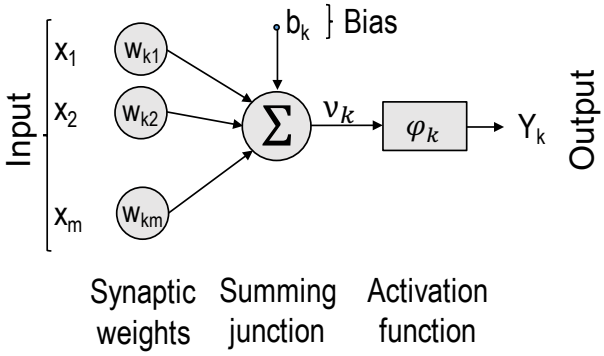

Figure 1. Scheme of a perceptron (or neurone)

The perceptrons (or neurones) (Fig. 1) are simple processing elements interconnected and layered. Each connection among neurons is weighted (synaptic weights, w). Hence, each neurone computes a weighted sum (a summing junction) based on the input variables values and a bias element (b). A

transfer function (φ) allows determining the output of the neurone as a result of the input weighted sums. The ANN realisation requires defining inputs, type of network, topology, training paradigm and transfer function. The ANN modelling allows for carrying out the required output starting from corresponding input vectors without considering the assumption of any determinate relationship between the input and output. There are many types of connection for the data transfer: the most used is the multi-layer perceptron (MLP). MLP is a feed-forward ANN where data flow from the input layer to the output layer through a different number of hidden layers without any feedback loop. The hidden layers represent the network computation model core. MLP networks can learn complex relationships between input and output patterns, and they show a better approximation of the constants allowing a quick link between steady and unsteady input values.

In the mathematical theory of the ANNs, the universal approximation theorem states that a feed-forward network, having a single hidden layer containing a finite number of neurones (i.e., a multilayer perceptron), can approximate continuous functions on compact subsets of $\mathbb{R}^n$ (real coordinate space) under mild assumptions on the activation function (Hornik et al., 1990). The theorem thus states that simple neural networks can represent a wide variety of interesting functions when given appropriate parameters. In particular, let φ be a non-constant, bounded, and monotonically-increasing continuous function; let I_m denote the m-dimensional unit hypercube $[0,1]^m$. The space of continuous function on I_m is indicated by $C(I_m)$. Then, given any function $y \in C(I_m)$ and $\varepsilon > 0$, there exists an integer N, real constants $b_i <\in \mathbb{R}$ and real vectors $w_i \in \mathbb{R}^m$, where i = 1,….,N, such that it can define:

$$Y(x) = \sum_{i=1}^{N} \varphi(w_i^T x + b_i) \quad (1)$$

as an approximate realisation of the function y, that is,

$$|Y(x) - y(x)| < \delta. \quad (2)$$

The most popular criteria used for measuring the performance of the ANNs are the absolute fraction of variation (R^2) and the mean square error (MSE). (The appendix A.1 reports their definition).

With the aim to configure the layout of an ANN, the main choices are related to the training algorithm, the number of hidden layers, the hidden neurones, and the transfer functions. The most selected learning rule for an MLP is the Error Back-Propagation (BP) algorithm (Khadse et al., 2016; Marquardt, 1963). This calculates the gradient of the network error in relation to its modifiable weights. The BP optimises the weight connection by allowing the error to spread from the output layers towards the lower layers (hidden layer and input layer). The network output is compared with the desired output and errors are computed. These errors are then back-propagated by adjusting the

weight such that the errors decrease with each iteration and the ANN model approximates the desired output. The network is trained to achieve an error goal of 10^{-6}. This typical problem, which occurs when the ANN is developing, is solved using cross-validation, which is a validation technique used to estimate how a model generalises an independent data set. In particular, the k-fold cross-validation method is applied to calculate the MSE, and the result can be used to select the best set of ANN parameters. Hence, the cross-validation is used to choose the best model between different plausible ANN alternatives. The number of hidden layers and the optimum number of hidden neurones may vary depending on the accuracy required. The number of neurones in the hidden layer and the number of hidden layers are optimised by trial and error to achieve accurate results (Mohanraj et al., 2011; Sheela and Deepa, 2013). However, regarding the number of the hidden neurones, an empirical rule may be considered (Hunter et al., 2012; Qian and Yong, 2013):

$$N_{hn} = 2N_i + 1 \,. \tag{3}$$

For the transfer functions, the best solution for the output layer is a linear function, while, because of the non-linearity problem, the best transfer function for the hidden layer is nonlinear (Cybenko, 1989). The most nonlinear selected functions are the sigmoid or hyperbolic tangent because their derivatives simplify the application of the BP algorithm.

3. The experimental setup and the test procedures

All data employed to build the ANN have been collected by designing a test set to carry out the energy performances of an actual magnetic refrigerator operating under different conditions. The device used is 8Mag, a permanent magnetic rotary refrigerator designed and built at University of Salerno (Aprea et al., 2014). Its magnetic system is based on a double U configuration of permanent magnets, and it performs a peak flux density of 1.25 T when the air gap is equal to 43 mm. Gadolinium is selected as a magnetic refrigerant, and demineralized water is employed as regenerating fluid. The total mass of gadolinium (1.20 kg), shaped as packed bed spheres (of 400÷500 μm), is confined within eight static regenerator enclosures, which are alternatively magnetised and demagnetized with the rotation of the magnets. Each regenerator has a height of 20 mm, a length of 45 mm, and a width of 35 mm. The volume available for the MCM is 31.5 cm^3. Considering the hydraulic diameter of the regenerator its aspect ratio is equal to 1.78. A rotary valve, mechanically coupled with the magnetic system, imparts the direction of the water through the regenerators. The cycle frequency (f_{AMR}) is determined by rotating the magnets; specifically, for each rotation of the magnets (n_{rpm}), each regenerator experiences two AMR cycles. A hydraulic system obtained by the combination of a rotary

valve and a vane pump ensures the proper distribution of the regenerating fluid in each component of the apparatus in agreement with the AMR cycle phases. The total fluid flow rate entering in the rotary valve is partitioned into two equal shares and then is transported to the regenerators. At each instant, there are four regenerators hydraulically connected to each other that are subject to the fluid flow: a couple is magnetised, and another one is demagnetized. At the same time, the remaining four regenerators are disconnected from the hydraulic circuit to experiment with their adiabatic temperature change. Based on the design specifications, the ratio between the magnetisation period and the fluid flowing period is 1:1 and their duration is imposed by the rotational speed of the magnets. The drive system consists of a brushless DC motor rotating the magnets at a variable speed between 0.1-1 Hz. A digital encoder and a programmable speed controller complete the drive system. The available maximum torque is equal to 70 Nm at 54 rpm. A photo of 8Mag is shown in Fig. 2.

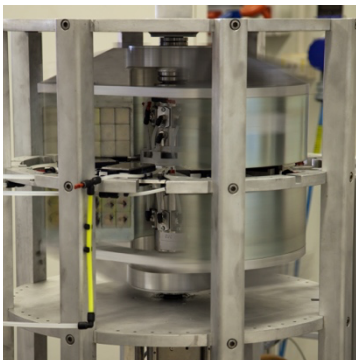

Fig. 2 Picture of the RPMMR prototype named 8Mag

Using PT100 thermo-resistances placed between the input and output of each component, the temperature of the regenerating fluid is measured. In particular:

- the temperature span (ΔT_{span}) is the average between the temperature of the regenerating fluid exiting the hot side (T_{HFo}) and the temperature of the regenerating fluid exiting the cold side (T_{LFo});
- the temperature of heat rejection (T_H) is the average time between the temperature of the water exiting the hot side of the magnetic refrigerator (T_{HFo}) and the water entering the hot side of the regenerator (T_{HFi}), both measured under steady state condition.

By using a magnetic flow meter placed between the pump and the hot heat exchanger, the volumetric flow rate of the regenerating fluid ($\dot{V}_f$) is measured. To estimate the pressure drops through the entire device, two piezoelectric pressure sensors placed between the input and the output of the pump are employed. The total pressure loss is evaluated as the average time over the difference between the pressure at the outlet (P_{out}) and the pressure at the inlet of the pump (P_{in}). The pressure measurements are also performed at the ends of the regenerators, with the objective of measuring the

blow duration and the pressure drop through the regenerators. The measurement of the utilisation factor (UF) was performed in agreement with the definition reported in (Tura and Rowe, 2011):

$$UF = \frac{M_f c_f}{M_{MCM} c_{MCM}} \quad (4)$$

where the fluid mass (M_f) over one blow period has been measured in the following manner:

$$M_f = \int_{\vartheta_i}^{\vartheta_f} \rho_f \dot{V}_f(\vartheta) d\vartheta \quad (5)$$

where $\dot{V}(\vartheta)$ is the fluid flow rate reported as a function of the rotation angle of the magnets θ, θ_f is the rotation angle for which the fluid is stopped and θ_i is the rotation angle for which the fluid start to blow through the regenerator. Further details are reported in (Aprea et al., 2014).

Using the digital encoder on the motor, the AMR cycle frequency is also measured. The test apparatus is equipped with 32 bit A/D converter acquisition cards with a sampling rate of up to 10 kHz. To measure the refrigeration duty provided by 8Mag, a cold heat exchanger has been realised by the combination of electric resistance with a thermally insulated pressure vessel. A variable voltage supply feeds the electrical resistance to provide a thermal load that is variable from 0 to 500 W. The T_H is adjusted by an electrical heater managed by a PID controller. In this way, under steady state conditions, it is possible to consider the following equation to be valid:

$$\dot{Q}_{ref} = \dot{W}_{el,h} \quad (6)$$

where $\dot{W}_{el,h}$ is the electrical power that made by the electric heater inserted into the heat exchanger and measured using a watt transducer. Using a PT100, temperature measurements on the outer surface of the insulation coat of the heat exchanger are performed to verify the quality of the insulation level. Moreover, using two transducers, the electrical power absorbed by the pump ($\dot{W}_p$) and the electrical power consumed by the electric motor used for magnet rotation ($\dot{W}_m$) are evaluated. For the evaluation of the COP, the following equation is used:

$$COP = \frac{\dot{Q}_{ref}}{\dot{W}_m + \dot{W}_p} = \frac{\dot{W}_{el,h}}{\dot{W}_m + \dot{W}_p} \quad (7)$$

In Table 1, the characteristics of the sensors used and the accuracy of the measurements performed particularly.

With the aim to define an operating map for 8Mag, a set of experiments has been designed and carried out by changing the following parameters: the T_H, the $\dot{W}_{el,h}$, the $\dot{V}_f$, and the n_{rpm}. Three T_H (16°C, 22°C, and 32 °C) as the hot thermal reference, and for each of them, a set of experiments were

carried out for different values of the $\dot{V}_f$ and the n_{rpm}. Because the vane pump is driven by an inverter, a set of three $\dot{V}_f$ values (5.0 l min^{-1}, 6.0 l min^{-1}, and 7.0 l min^{-1}) were employed. Consequently, the n_{rpm} were selected so that, for each $\dot{V}_{f,r}$ value experimented, the UF was equal to the following values: 2.70, 1.80, 1.30, 0.87, and 0.52. Finally, for each test condition, different values of the thermal load were imposed: by starting under the zero load condition, the maximisation load was incremented until ΔT_{span} was greater than zero. In this way, 180 experiments were collected in agreement with the operational limits both of the pump and of the electrical motor.

4. ANNTEO

ANNTEO (Artificial Neural Network Technique for Energy Optimisation) is a technique to control the cooling capacity of an RPMMR as a function of the operating conditions of the refrigerator and the requests from the user. The purpose of the control is not only the definition of an operating point, ensuring the matching of supply and demand, but also the identification of the optimum operating point regarding:

- The maximum COP, and then an energy saving;
- The maximum cooling capacity, obtaining a time-saving. In fact, for an individual thermal load, if the system can work at its maximum cooling capacity, the difference between the supply and the demand will be larger, and then the device takes less time to achieve the thermal set point.

The following describes in detail the concept on which ANNTEO is based, the ANN that allows the implementation of ANNTEO, and the finding process of the optimum operating conditions.

Quantity	Characteristic	Accuracy
Temperature	RTD PT100	± 0.1 [K]
Pressure	Piezoelectric Pressure gauge	± 75 [kPa]
Volumetric flow rate	Electromagnetic Flowmeter	± 0.5%
Rpm / Frequency	Optical Encoder	± 0.01 [° s $^{-1}$]
Mass	Electronic Balance	± 0.2 [g]
Electrical power	Electromagnetic Wattmeter	± 0.2%
Torque	Torque transducer	± 0.5%
UF	Procedure introduced in (Aprea et al., 2014)	±5.3%
COP	Eq. 2 & Propagation Error Analysis	±0.35%

Table 1. Characteristics of the sensors used and the accuracy of the measurements performed.

4.1. The concept

Several authors have identified the f_{AMR}, the $\dot{V}_f$ and the T_H can influence the performances of a magnetic refrigerator. The first two conditions can be referred to as internal operating conditions because related to the operation of the system employed. Otherwise, considering a real application in which a magnetic refrigerator provides the cooling power to a fridge, the temperature of rejection is imposed from the outside (ambient temperature), for which it is defined as operating external condition and is not controllable. Consequently, the degrees of freedom available to control the operation of a magnetic refrigerator are only two. In particular, concerning the rotor systems, the real internal operating conditions are the the number of revolutions of the magnets or the regenerators per minute and the volumetric flow of the regenerating fluid. As shown in the literature, the relationships that exist between the internal operating conditions and the performance of a system are not linear. Moreover, as predicted by the theory for certain operating conditions differs considerably from the reality because of the special construction taken in the different existing prototypes and that lead to problems difficult to be modelled and highly varied. This observation, together with the burden of calculation, which characterises the theoretical models, leads to consider the traditional modelling little suitable to build a controller. To overcome this problem, for each type of system a map of operation should be identified experimentally under different operating conditions (internal and external).Wanting to take advantage of an accurate and robust system (able to know how to handle every situation), it is easy to understand that experimental mapping could be costly in both economic and temporal terms. For these reasons, the development of a control technique for a PMMR may be facilitated by the use of ANNs. The idea, then, is to develop a constrained optimisation algorithm that takes as input a map of points of operation provided by an ANN trained with a reduced amount of experimental data. As a consequence, the ANN represents the heart of the whole process. In Fig.3 it is shown the flow chart under which ANNTEO operates.

The process begins by receiving in input:

- The demand data regarding the desired temperature within the volume to be cooled ($T_{SET\ point}$) and the hot source temperature (T_H). Consequently, the ΔT_{span} required to the magnetic refrigerator will be greater than the difference between T_H and $T_{SET\ point}$ of a quantity dependent on the characteristics of the heat exchangers used such as links between the machine and the user (the cold side, ΔT_{CHX}) and between the machine and the hot source (hot side, ΔT_{HHX}):

$$\Delta T_{SET} = (T_H + \Delta T_{HHX}) - \left(T_{SET,point} - \Delta T_{CHX} \right) \quad (8)$$

- The domain of the internal operating conditions identified by considering the operating limits of the electric motor used for the rotation of the magnets and the pump used for the circulation of the regenerating fluid.

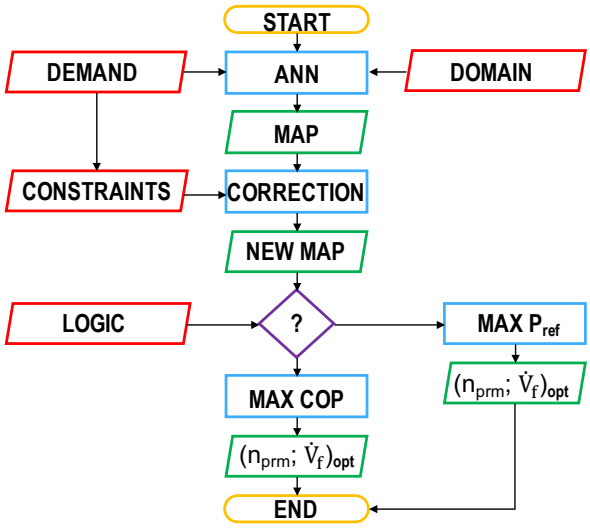

Fig. 3 ANNTEO's flow chart

The inputs are processed by the ANN which provides in output a first operating map having more dimensions and showing the energy performance for each pair of permissible internal operating conditions. At this point, the map is intersected with the constraints that are expressed concerning minimum required cooling capacity as a function of the thermal load. This value can be either fixed or changeable so as to determine a descent ramp of the temperature inside the fridge and able to satisfy different requirements (such as a rapid cooling or a keeping of the temperature). The application of the constraints to the map leads to a new map which corresponds to a new domain of the internal operating conditions. Then the user can select the logic optimisation choosing between maximum cooling capacity and maximum COP. In both cases, a maximisation process is applied that leads to the definition of the optimum pair of the internal operating conditions In particular, adopting the logic of the maximisation of the cooling capacity, ANNTEO establishes the operational strategy for the magnetic refrigerator such as to minimise the cooling time and exceeding the minimum required cooling power limit, while, by adopting the logic of maximising the COP, ANNTEO ensures the energy saving compatible with the thermal load.

4.2. The ANN: design, training and performances

The ANN adopted in ANNTEO is an MLP feed-forward type having a hidden layer, four input neurones and four output neurones (Fig. 4). The inputs are associated with the internal operating conditions ($\dot{V}_f$ and n_{rpm}), the user request (ΔT_{SET}) and the external operating condition (T_H). The outputs are the achievable energy performances: the $\dot{Q}_{ref}$, the $\dot{W}_m$, the $\dot{W}_p$, and the COP. In particular, for a generic pair of ΔT_{SET} and T_H, the inputs can be organised in the following matrix

$$Input^{\langle \Delta T^p, T^q \rangle} = \begin{bmatrix} (\dot{V}_{f,1}; n_{rpm,1}; \Delta T^p; T^q) & \cdots & (\dot{V}_{f,h}; n_{rpm,1}; \Delta T^p; T^q) \\ \vdots & \boldsymbol{input}_{kj}^{\langle \Delta T^p, T^q \rangle} & \vdots \\ (\dot{V}_{f,1}; n_{rpm,m}; \Delta T^p; T^q) & \cdots & (\dot{V}_{f,h}; n_{rpm,m}; \Delta T^p; T^q) \end{bmatrix} \quad (9)$$

where: $\dot{V}_{f,1}$and $\dot{V}_{f,h}$ are respectively the minimum and the maximum volumetric flow rate process processable by the pump; $n_{rpm,1}$ and $n_{rpm,m}$ are respectively the minimum and maximum number of revolutions obtained by means of the electric motor; ΔT^p is a generic value of the temperature span included in the following array:

$$\Delta T_{SET} = \{0; \dots; \Delta T(\dot{Q}_{ref} = 0)\}; \quad (10)$$

T^q is a generic value of the hot source temperature between the minimum temperature ($T_{H,\,min}$) and the maximum temperature ($T_{H,\,max}$) of the environment.

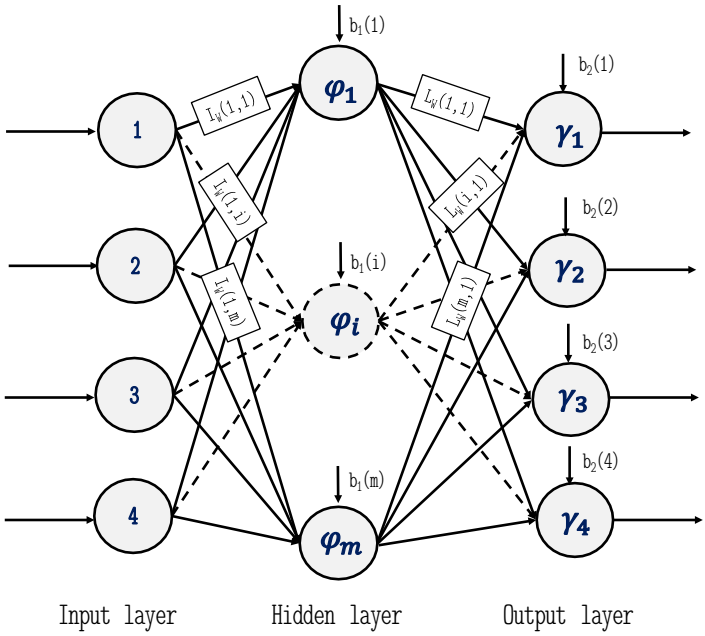

Fig. 4 the adopted ANN structure

Considering the morphology of the ANN, one can transcribe the mathematical formulation of the ANN as follows:

$$Y^{\langle \Delta T^p, T^q \rangle} = \gamma[\bar{L}_W \times \left[\varphi\left(\bar{I}_W \times \boldsymbol{input}_{kj}^{\langle \Delta T^p, T^q \rangle} + \boldsymbol{b}_1\right)\right] + \boldsymbol{b}_2] \quad (11)$$

where $\bar{L}_W$ is the matrix of weights of the output neurones, $\bar{I}_W$ is the matrix of weights of the hidden neurones, $\boldsymbol{b}_1$ is the vector of the biases at the hidden layer, $\boldsymbol{b}_2$ is the vector of the biases to the output layer, φ is the transfer function in the hidden layer, and γ is the transfer function in the output layer. In particular, the hidden layer adopts the sigmoidal transfer functions, while the linear functions are the transfer function in the output layer:

$$\begin{cases} \varphi = \frac{1-e^{-2\beta}}{1+e^{-2\beta}} \\ \gamma = \varphi \end{cases} , \beta = \bar{I}_W \times \boldsymbol{input}_{\boldsymbol{kj}}^{\langle \Delta T^p, T^q \rangle} + \boldsymbol{b}_1 \quad . \tag{12}$$

For each element of the input array, the ANN processes an output vector. Consequently, organising all the output vectors in a matrix, one can obtain the following multidimensional map:

$$\bar{Y}^{\langle \Delta T^p, T^q \rangle} = \begin{Bmatrix} \overline{\dot{Q}_{ref}} \\ \overline{\dot{W}_m} \\ \overline{\dot{W}_p} \\ \overline{COP} \end{Bmatrix} = \left\{ \begin{bmatrix} \dot{Q}_{ref,11} & \cdots & \dot{Q}_{ref,1j} \\ \vdots & \ddots & \vdots \\ \dot{Q}_{ref,k1} & \cdots & \dot{Q}_{ref,kj} \end{bmatrix} \begin{bmatrix} \dot{W}_{m,11} & \cdots & \dot{W}_{m,11} \\ \vdots & \ddots & \vdots \\ \dot{W}_{m,11} & \cdots & \dot{W}_{m,11} \end{bmatrix} \begin{bmatrix} \dot{W}_{p,11} & \cdots & \dot{W}_{p,1j} \\ \vdots & \ddots & \vdots \\ \dot{W}_{p,k1} & \cdots & \dot{W}_{p,kj} \end{bmatrix} \begin{bmatrix} COP_{11} & \cdots & COP_{1j} \\ \vdots & \ddots & \vdots \\ COP_{k1} & \cdots & COP_{kj} \end{bmatrix} \right\}. \tag{13}$$

Concerning the number of neurones in the hidden layer, the Eq. (3) has suggested the adoption of nine hidden neurones. However, following the suggestions of the literature (Mohanraj et al., 2011; Sheela and Deepa, 2013), a trial and error analysis has led to the choice of 11 hidden neurones (the appendix A.2 reports the results of the analysis).

The first step for the network training has been to define the training set. By starting from the data obtained with the experimental campaign (see section 3), a subset of 108 experiments composed the training set. At this point, it was considered a subsystem of the training set (validation set) consisting of 54 tests and a further subsystem consisting of 10 experiments (test set). The validation set was used for the finding of synaptic weights using the Levenber-Marquardt algorithm, which has been applied along with methods of early stopping cross-validation to avoid the over-fitting problem and to test the generalisation ability of the ANN. As suggested by (Jayalakshmi and Santhakumaran, 2011), before to start with the training of the ANN, the available experimental data have been appropriately normalised in the range of values between -1 and 1. The generation of the network and the learning algorithm implementation were performed with the help of the Neural Network Tool

available in Matlab. With the aim to not make the network affected by the date used as training set, they have been chosen by means of a random extraction routine. Several extractions were performed, and a new network was generated for each of them. Among all the networks generated both the MSE and the R^2 showed slight changes.

Following the training process (the appendix A.3 reports the matrixes of the synaptic weights and the array of the biases) the ANN designed was validated as a result of a comparison between the experimental data of the validation set and the test set respectively. As shown in Fig. 5, for each of the output variables of the ANN it is possible to highlight a good agreement between the predicted and the experimental data. In particular, the ANN has recorded an MSE included in the range 0.0049-0.0054 and an R^2 included in the range 0.09821-0.9939.

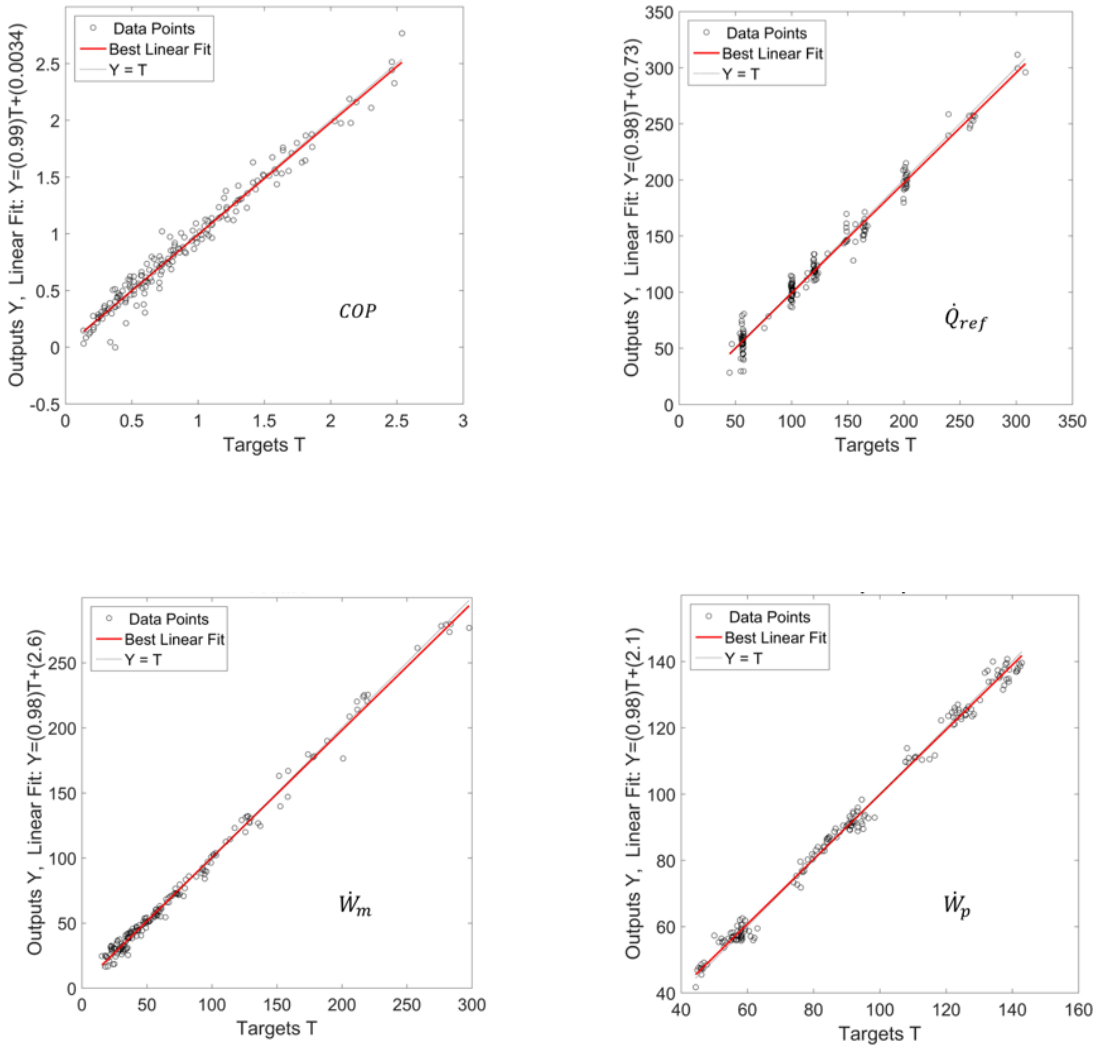

Fig. 5 Results of the ANN validation. Targets (T) represent the experimental data vs the outputs of the ANN (Y)

These results show the ANN can predict with a good level of confidence the energy performances also in those operating conditions to it not known. Consequently, the domain of existence of the ANN can be extended from the discreet, represented by the Eq. (6), to a continuous type:

$$\boldsymbol{x} \in \mathbb{D}_{in} = \mathbb{R}^4 - \left\{ \begin{array}{ccc} \dot{V}_f < \dot{V}_{f,1} & \wedge & \dot{V}_f > \dot{V}_{f,h} \\ n_{rpm} < n_{rpm,1} & \wedge & n_{rpm} < n_{rpm,k} \\ \Delta T_{SET} < 0 & \wedge & \Delta T_{SET} > \Delta T(\dot{Q}_{ref} = 0) \\ T_H < T_{H,min} & \wedge & T_H > T_{H,max} \end{array} \right\} \tag{14}$$

In this way, the ANN designed here resumes the representation introduced in Eq. (1):

$$\boldsymbol{Y} = Y\left(\dot{V}_f, n_{rpm}, \Delta T_{SET}, T_H\right) \tag{15}$$

returning a vector of surfaces, each for every output of the ANN.

4.3. The optimisation process

The formulation of the ANN by the Eq. (13) allows to quickly find the pair of the operating conditions able to satisfy the desired operating logic: maximum COP or maximum refrigeration power. Consistent with the operational constraints of the specific application, in both cases, it is necessary to resort to the constrained optimisation process applied to the ANN. Considering went as shown in the diagram in Fig. 3, one must first impose a constraint on the minimum required power ($\dot{Q}_{req}$):

$$\boldsymbol{Y}_{con} = \boldsymbol{Y} + \left\{-\dot{Q}_{req}; 0; 0; 0\right\}^T \tag{16}$$

This causes a downward offset of the entire surface $\dot{Q}_{ref}$; consequently, all the pairs of operating conditions, for which the actual refrigerating capacity is less than the $\dot{Q}_{req}$ will return a value of cooling capacity equal to 0W.

Later formulations of the optimisation problem are identified:

Maximisation of the cooling capacity

$$\begin{cases} max\ Y_{con,1}(\boldsymbol{x}) \\ Y_{con,1}(\boldsymbol{x}) \geq 0 \\ \boldsymbol{x} \in \mathbb{D}_{in} \\ \Delta T_{SET} = \Delta T_{req} \\ T_H = T_{H,req} \end{cases} \tag{17}$$

Maximisation of the COP

$$\begin{cases} max\ Y_{con,4}(\boldsymbol{x}) \\ Y_{con,1}(\boldsymbol{x}) \geq 0 \\ \boldsymbol{x} \in \mathbb{D}_{in} \\ \Delta T_{SET} = \Delta T_{req} \\ T_H = T_{H,req} \end{cases} \tag{18}$$

where $Y_{con,1}$ and $Y_{con,4}$ represent respectively the surfaces of the cooling capacity and the COP, and ΔT_{req} and $T_{H,req}$ the values of the external operating conditions. The identification of the optimal operating conditions is guaranteed by the Optimisation Toolbox Matlab operating with the algorithm of the interior point.

5. Results

To show the results obtainable by means of ANNTEO, it is appropriate to consider a practical case for which the external operating conditions are fixed, and the identification of the optimal operating conditions is required in both the maximum cooling capacity mode and the maximum COP mode. In this regard, a random situation, unknown to the ANN but such that the operating conditions can be included in the domain known to the ANN, has been considered. It is supposed to seek the optimum operating point for 8Mag when we need a ΔT_{SET} equal to 8 K and a minimum refrigeration power of 50 W, while the T_H is equal to 295 K. After the definition of such user demand, the domain of the internal operating conditions has been provided to ANNTEO:

$$\begin{matrix} 5\ l\ min^{-1} \leq \dot{V}_f \leq 7\ l\ min^{-1} \\ 10\ rpm < n_{rpm} \leq 55\ rpm \end{matrix} \tag{19}$$

At this point, in agreement with section 4.1, the ANN at the base of ANNTEO is able to provide the operating map (Fig. 6). However, such an operating map doesn't comply with the constraint of the minimum refrigeration power required for the practical case here examined.

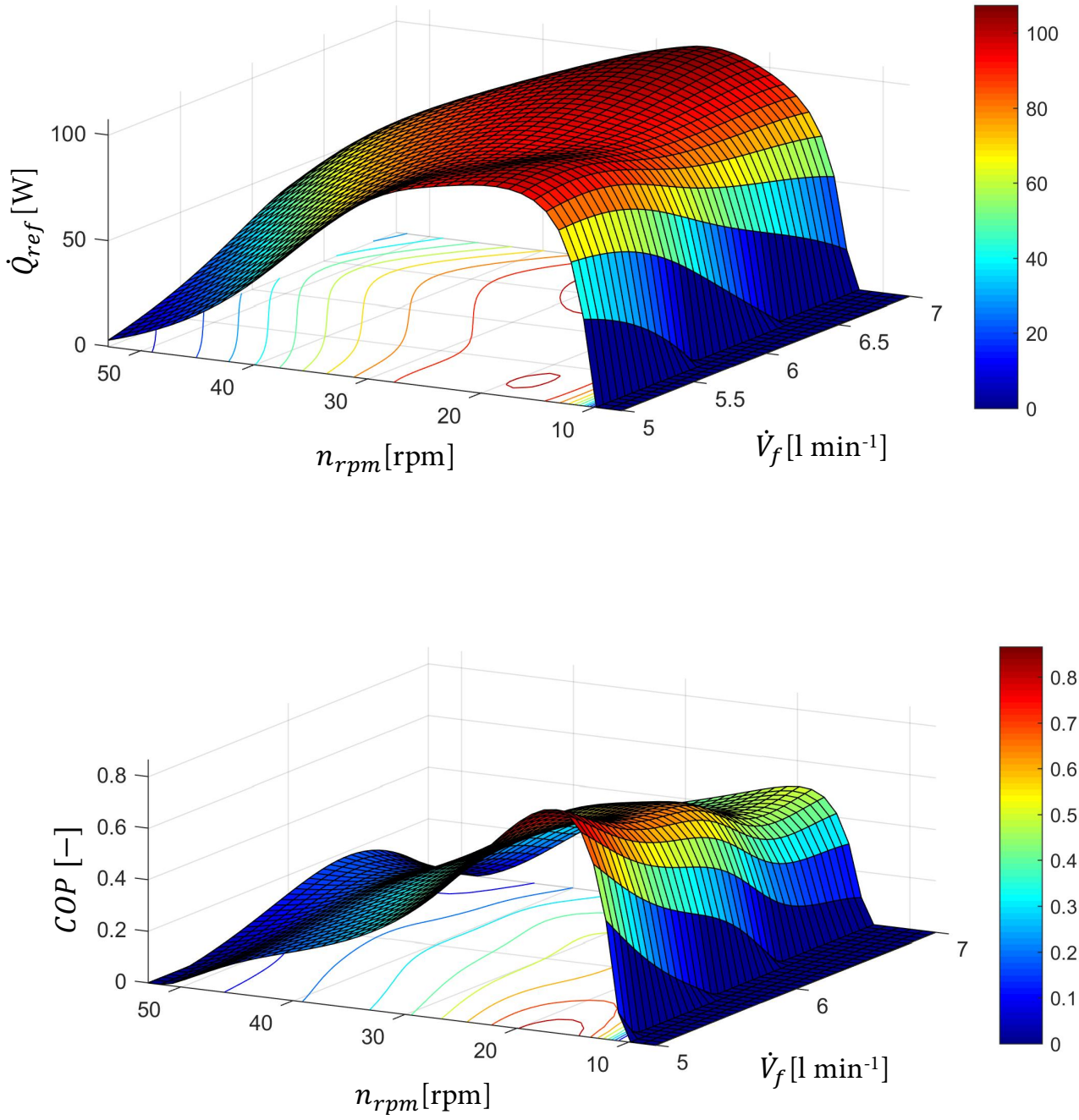

Fig. 6 Map of the $\dot{Q}_{ref}$ and of the COP generated by the ANN (ΔT_{SET}=8K and T_H=295K). The colour legend bar shows the correspondence between the colours and the values of the dimension on the z-axis.

Consequently, ANNTEO proceeds to correct the operating map, and then it subtracts the set of those operating conditions for which the refrigerator could not satisfy the constraints. In this manner, a new map is carried out (Fig. 7) and, in accordance with the Fig. 3, one of the optimisation logics can be applied. However, the optimisation process requires a thorough search, so applying the Eq.s 16,

17, and 18, it is possible to derive the optimal operating points (Fig. 7a and b): $\dot{Q}_{ref,max}$=107 W and COP = 0.42 at $(\dot{V}_f; n_{rpm})_{opt}$=(6.9 l min^{-1}; 26.4 rpm); $\dot{Q}_{ref}$=96 W and COP_{max} = 0.85 at $(\dot{V}_f; n_{rpm})_{opt}$=(5.0 l min^{-1}; 16.5 rpm).

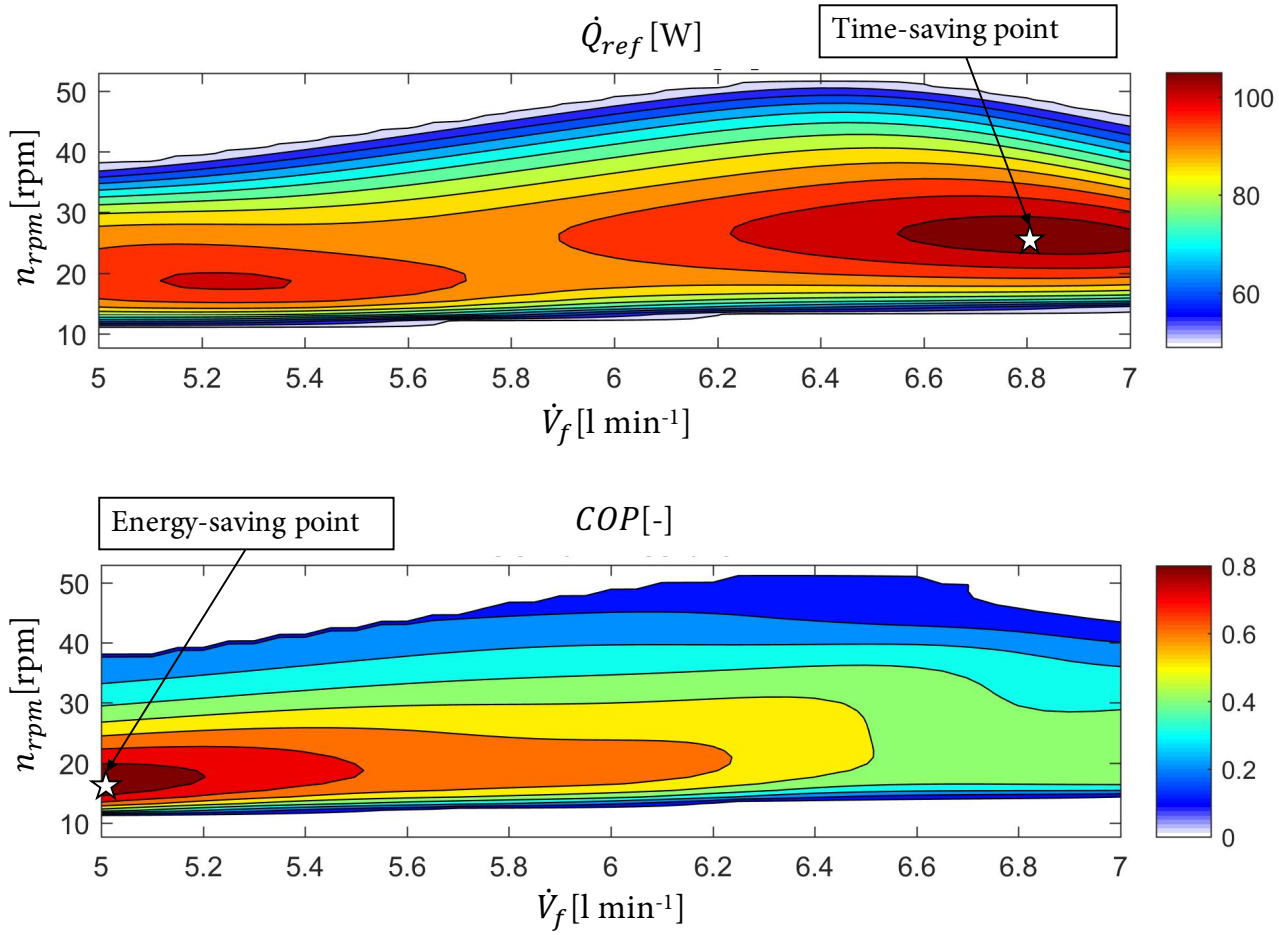

Fig. 7 The optimisation process obtained by ANNTEO. The white star shows the optimal operating conditions, while the white area represents the set of those operating conditions for which the refrigerator could not satisfy the constraints. The colour legend bar shows the correspondence between the colours and the values of the dimension on the z-axis.

The internal operating conditions carried out with the aid of ANNTEO were employed as test conditions to verify the goodness of the method, obtaining an acceptable deviation (Tab. 2).

Operating conditions	Experimental results	ANNTEO errors
$(\dot{V}_f, n_{rpm}, \Delta T_{SET}, T_H)$	$(\dot{Q}_{ref}$, COP)	$(\varepsilon_{\dot{Q}_{ref}}, \varepsilon_{COP})$
(6.8 l min^{-1}; 26.4 rpm; 8°C; 22°C)	(112 W; 0.38)	(-4 %; +9%)
(5.0 l min^{-1}; 16.5 rpm; 8°C; 22°C)	(92 W; 0.91)	(+4 %; -7%)

Tab. 2 Comparison between the experimental and the predicted data by ANNTEO.

With the aim to enforce the correctness of the ANN model at the base of ANNTEO, it is worthy to analyse the results reported in Fig. 6 by comparing the behaviour of 8Mag reproduced by the ANN with those of the magnetic refrigerators reported in the literature. As well in (Lozano et al., 2014; Trevizoli et al., 2016; Tušek et al., 2013b), the prediction of the ANN shows the presence of several local maxima in terms both of the optimal cycle frequency and of the optimal volumetric flow rate. Both the volumetric flow rate and cycle frequency influence the $\dot{Q}_{ref}$, causing a quick increasing of the refrigeration power for small $\dot{V}_f$ and n_{rpm} values, and a moderate decreasing for large $\dot{V}_f$ and n_{rpm} values. Also, with reference to Fig.7, there are several couples of $\dot{V}_f$ and n_{rpm} values for which the refrigeration power achieves the same value. That allows to select several internal operating conditions that compliance the user demand and then leads to an easier control of the device. Looking at the COP changing, it is noticeable a harder influence of the volumetric flow rate than of the cycle frequency. In particular, an increasing of the cycle frequency causes a decreasing of the COP, while by varying the $\dot{V}_f$ the COP shows an local maximum.

It is worthy to note this behaviour is due to the overlapping of different causes that can affect the performances of an actual magnetic refrigerator such as 8Mag (i.e. heat losses, dead volumes, regenerator efficiency, eddy currents) and that couldn't be predicted by means of the traditional modelling employed in the field of the magnetic refrigeration.

A further validation of the ANN model is awarded, as shown in Fig.8, where a direct comparison between the predicted and the measured values is depicted both for the $\dot{Q}_{ref}$ and the COP. The data were collected for three $\dot{V}_f$ values and for several n_{rpm}, considering the experimental data unknown to the ANN. The external operating conditions and the user demand were the same of the practical case introduced before. As shown in Fig. 8 a small difference is noticeable between the measured and the predicted values $\dot{Q}_{ref}$ (±5%), while a larger difference is observable for the COP values (±10%). However, Fig. 8 displays that ANNTEO provides a good accuracy in the prediction of the optimal internal operating conditions, then its main aim is satisfied.

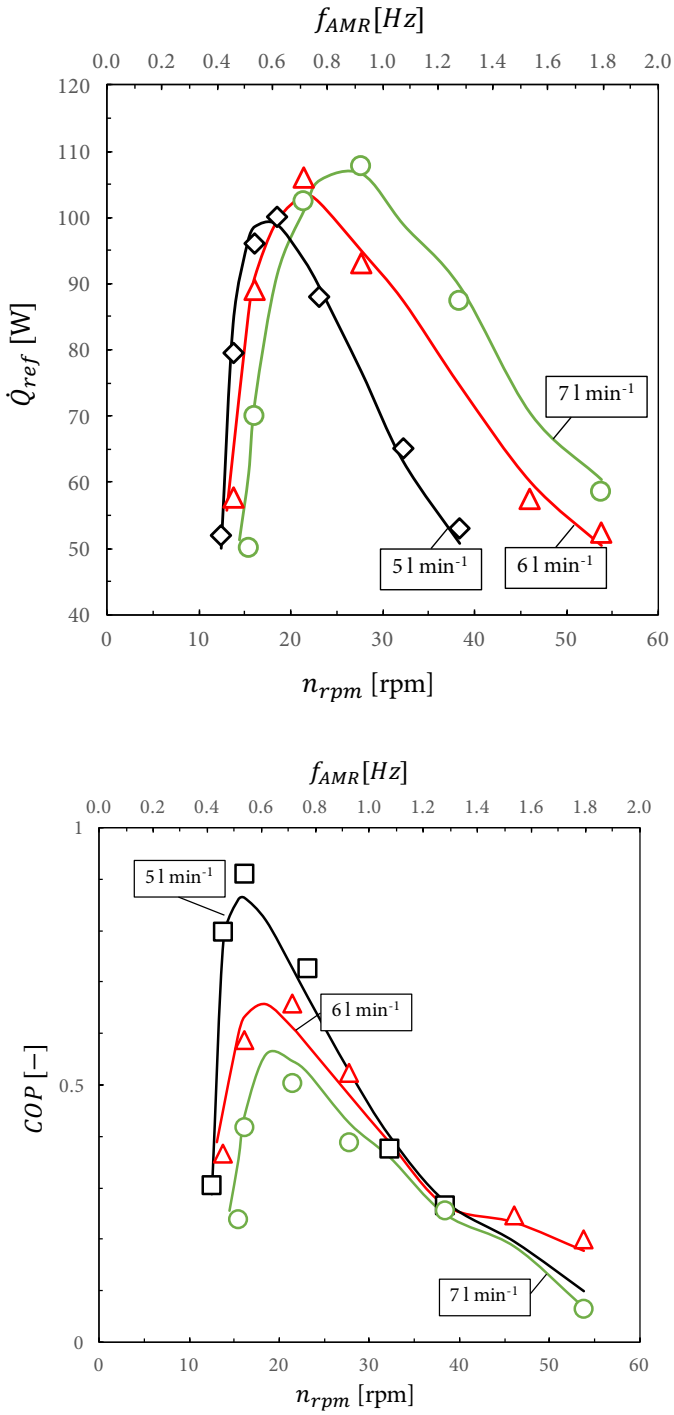

Fig. 8 Comparison between the predicted and the measured values. Continuous lines represent the predicted values, while the experiments are depicted using the symbols.

The results reported here by way of example have been obtained by implementing ANNTEO through a script designed in the Matlab environment and run on a personal computer. However, the technique is just implementable via a cheap and user-friendly electronic platform. Also, it is usable "on board" so as to provide, in real time, the internal operating optimal conditions for a magnetic refrigerator. In particular, ANNTEO could be either fully implemented on a controller to predict the

optimum operating conditions, or employed as the trainer of a most basic neural network dedicated only to the identification of the optimal operating conditions. The first solution, although costlier from a computational point-of-view, provides a more flexible tool. In fact, ANNTEO may be coupled to a self-learning procedure so as to expand its action domain in addition to that for which it was initially instructed and, at the same time, to refine its predictions. The second solution, instead, would be leaner from the computational point of view but very stiff.

6. Conclusions

This work has presented ANNTEO, a technique based on the use of neural networks and aimed at the optimisation of a magnetic refrigerator operating with permanent magnets. After introducing the concept of modelling a magnetic refrigerator using the ANN, it describes the procedure on which ANNTEO works. Therefore, it widely describes the phase of the design and the implementation and testing of that ANN, which by receiving in input both the internal and external conditions, can predict the energy performances of a PMMR. With the aim to prove the efficiency of ANNTEO, all results are referenced to the magnetic refrigerator prototype called 8Mag. After a trial and error analysis, the best architecture for the ANN was found to be an MLP type with a hidden layer having 11 neurones, 4 input neurones and 4 output neurones. The training phase was carried out using a training set composed of 108 experiments, of which 54 were used for the definition of the synaptic weights and 10 to test the neural network. The ANN showed good accuracy, quantified with an MSE included in the range 0.0049-0.0054 and an R^2 included in the range 0.09821-0.9939. After, the method of the optimisation was introduced. In particular, two operating modes have been described: maximum cooling capacity and maximum COP. With the aim to test the ANNTEO method, a random situation, unknown to the ANN but such that the operating conditions are included in the domain known to the ANN, has been considered. By way of example, ANNTEO has been employed to seek the optimum operating point for 8Mag when a ΔT_{SET} is needed equal to 8 K and a minimum cooling capacity of 50 W, while the T_H is equal to 295 K. The results obtained were employed as conditions of experimental tests designed to test the accuracy of ANNTEO, which showed an error less than +/- 10% for the COP and less than +/- 5% for the cooling capacity.

In conclusion, the results reported here lead to the following:

- The use of the ANN gives an accurate way to model a magnetic refrigerator as it is built.

- It is not a universal ANN that is effectual for any magnetic refrigerator, but it is possible to consider the MLP type as a global architecture.
- The realisation of ANNTEO requires a reduced number of experiments when compared with the usual experimental characterizations placed at the base of the traditional control systems.
- ANNTEO is capable of detecting internal operating conditions that maximise the cooling capacity or the COP.
- ANNTEO can be implemented on a programmable electronic card, or it can be employed as the trainer of a most basic ANN able only to find the optimal internal operating conditions.

It is worthy to observe that ANNTEO works efficiently if the operating conditions fall within the domain of training, while it is not able to extrapolate in front of operating conditions never seen. However, it is possible to overcome this problem by using a technique for self-training of the ANN used to predict the performance of the magnetic refrigerator. Future works will be used to implement ANNTEO on board and to develop a self-training algorithm.

7. Appendix

A.1 Performance of the ANN

The criteria used for measuring the performance of the ANN are the absolute fraction of variation (R^2) and the mean square error (MSE). The R^2 is given by the following equation:

$$R^2 = 1 - \frac{\sum_{m=1}^{n}(Y_m - y_m)^2}{\sum_{m=1}^{n}(y_m)^2} \quad \text{(A.1)}$$

while the MSE is calculated by

$$MSE = \frac{\sum_{m=1}^{n}(Y_m - y_m)^2}{n} \quad \text{(A.2)}$$

A.2 Trial and error analysis

The performance of the ANNs having different hidden neurone numbers are reported concerning MSE and R^2 as result of the trial and error analysis.

N_{hn}	MSE	R^2
9	0.0091	0.9871
10	0.0129	0.9847
11	0.0049	0.9939

12	0.0295	0.9618
13	0.011	0.9845
14	0.0053	0.9889
15	0.0118	0.9846
16	0.0073	0.9789

A.3 Synaptic weights and biases of the ANN

About Eq.9 in the text, the matrixes $\bar{L}_W$ and $\bar{I}_W$ (synaptic weights) and the arrays b1 and b2 (biases) of the ANN used in the present work are the following:

$\bar{I}_W$	**input 1**	**input 2**	**input 3**	**input 4**
h1	-0.457	-1.056	-0.450	-0.086
h2	-0.199	0.691	0.493	0.326
h3	-0.388	-0.062	-0.757	1.406
h4	-0.457	-0.511	0.152	0.281
h5	2.015	-0.111	-1.041	-0.168
h6	0.174	-0.980	-0.051	0.026
h7	0.557	0.508	-0.183	0.104
h8	1.805	0.156	0.390	0.198
h9	-1.274	-1.819	-0.625	0.176
h10	-0.463	1.332	0.190	-1.766
h11	-0.331	6.591	-0.939	0.029

$\bar{L}_W$	**h1**	**h2**	**h3**	**h4**	**h5**	**h6**	**h7**	**h8**	**h9**	**h10**	**h11**
output 1	1.121	-1.697	0.660	-1.131	-0.311	1.210	0.924	-0.519	-0.286	0.165	3.140
output 2	0.949	0.585	0.122	-0.471	0.015	-1.047	-0.292	0.122	-0.328	-0.052	0.039
output 3	-1.322	-0.672	-0.290	-0.047	0.233	0.131	0.011	0.465	0.406	0.166	-0.317
output 4	2.513	-1.114	0.384	-0.197	-0.003	0.418	0.145	-0.131	-0.269	0.115	3.353

b1,1	-2.069
b1,2	1.811
b1,3	2.273
b1,4	0.426
b1,5	-0.087
b1,6	0.349
b1,7	0.350
b1,8	-0.013
b1,9	-2.766
b1,10	1.159
b1,11	6.680

b2,1	-2.354
b2,2	0.216
b2,3	0.104
b2,4	-1.398

Aprea, C., Greco, A., Maiorino, A., 2015. GeoThermag: A geothermal magnetic refrigerator. Int. J. Refrig. 59, 75–83. doi:10.1016/j.ijrefrig.2015.07.014

Aprea, C., Greco, A., Maiorino, A., Mastrullo, R., Tura, A., 2014. Initial experimental results from a rotary permanent magnet magnetic refrigerator. Int. J. Refrig. 43, 111–122. doi:10.1016/j.ijrefrig.2014.03.014

Bahl, C.R.H., Engelbrecht, K., Eriksen, D., Lozano, J.A., Bjørk, R., Geyti, J., Nielsen, K.K., Smith, A., Pryds, N., 2014. Development and experimental results from a 1 kW prototype AMR. Int. J. Refrig. 37, 78–83. doi:10.1016/j.ijrefrig.2013.09.001

Bahl, C.R.H., Navickaitė, K., Neves Bez, H., Lei, T., Engelbrecht, K., Bjørk, R., Li, K., Li, Z., Shen, J., Dai, W., Jia, J., Wu, Y., Long, Y., Hu, F., Shen, B., 2017. Operational test of bonded magnetocaloric plates. Int. J. Refrig. doi:10.1016/j.ijrefrig.2017.02.016

Benedict, M.A., Sherif, S.A., Schroeder, M., Beers, D.G., 2017a. Experimental impact of magnet and regenerator design on the refrigeration performance of first-order magnetocaloric materials. Int. J. Refrig. 74, 190–199. doi:10.1016/j.ijrefrig.2016.09.023

Benedict, M.A., Sherif, S.A., Schroeder, M., Beers, D.G., 2017b. The impact of magnetocaloric properties on refrigeration performance and machine design. Int. J. Refrig. 74, 576–583. doi:10.1016/j.ijrefrig.2016.12.004

Bjørk, R., Bahl, C.R.H., Nielsen, K.K., 2016. The lifetime cost of a magnetic refrigerator. Int. J. Refrig. 63, 48–62. doi:10.1016/j.ijrefrig.2015.08.022

Bjørk, R., Smith, A., Bahl, C.R.H., Pryds, N., 2011. Determining the minimum mass and cost of a magnetic refrigerator, in: International Journal of Refrigeration. pp. 1805–1816. doi:10.1016/j.ijrefrig.2011.05.021

Bouchekara, H.R.E.H., Kedous-Lebouc, A., Yonnet, J.P., Chillet, C., 2014. Multiobjective optimization of AMR systems. Int. J. Refrig. 37, 63–71. doi:10.1016/j.ijrefrig.2013.09.009

Coulomb, D., 2016. Thermag VII – magnetic refrigeration is gaining ground. Int. J. Refrig. 72, v–vi. doi:10.1016/j.ijrefrig.2016.10.005

Cybenko, G., 1989. Correction: Approximation by Superpositions of a Sigmoidal Function. Math. Control. Signals, Syst. 2, 303–314. doi:doi: 10.1007/BF02134016

Eriksen, D., Engelbrecht, K., Bahl, C.R.H., Bjørk, R., Nielsen, K.K., 2016. Effects of flow balancing on active magnetic regenerator performance. Appl. Therm. Eng. 103, 1–8. doi:10.1016/j.applthermaleng.2016.03.001

Hornik, K., Stinchcombe, M., White, H., 1990. Universal approximation of an unknown mapping and its derivatives using multilayer feedforward networks. Neural Networks 3, 551–560. doi:10.1016/0893-6080(90)90005-6

Hunter, D., Yu, H., Pukish, M.S., Kolbusz, J., Wilamowski, B.M., 2012. Selection of Proper Neural Network Sizes and Architectures — A Comparative Study. IEEE Trans. Ind. Informatics 8, 228–240. doi:10.1109/TII.2012.2187914

Jayalakshmi, T., Santhakumaran, a, 2011. Statistical normalization and back propagation for classification. Int. J. Comput. … 3, 1–5.

Khadse, C.B., Chaudhari, M.A., Borghate, V.B., 2016. Conjugate gradient back-propagation based artificial neural network for real time power quality assessment. Int. J. Electr. Power Energy Syst. 82, 197–206. doi:http://dx.doi.org/10.1016/j.ijepes.2016.03.020

Kitanovski, A., Tušek, J., Tomc, U., Plaznik, U., Ožbolt, M., Poredoš, A., 2015. Overview of Existing Magnetocaloric Prototype Devices, in: Magnetocaloric Energy Conversion: From Theory to Applications. Springer International Publishing, Cham, pp. 269–330. doi:10.1007/978-3-319-08741-2_7

Lei, T., Engelbrecht, K., Nielsen, K.K., Veje, C.T., 2015. Study of geometries of active magnetic regenerators for room temperature magnetocaloric refrigeration. Appl. Therm. Eng. doi:10.1016/j.applthermaleng.2015.11.113

Lozano, J.A., Capovilla, M.S., Trevizoli, P. V., Engelbrecht, K., Bahl, C.R.H., Barbosa, J.R., 2016. Development of a novel rotary magnetic refrigerator. Int. J. Refrig. 68, 187–197. doi:10.1016/j.ijrefrig.2016.04.005

Lozano, J.A., Engelbrecht, K., Bahl, C.R.H., Nielsen, K.K., Barbosa, J.R., Prata, A.T., Pryds, N., 2014. Experimental and numerical results of a high frequency rotating active magnetic refrigerator. Int. J. Refrig. 37, 92–98. doi:10.1016/j.ijrefrig.2013.09.002

Marquardt, D.W., 1963. An algorithm for least-squares estimation of non-linear parameters. J. Appl. Math. 11, 531–444.

Mohanraj, M., Jayaraj, S., Muraleedharan, C., 2011. Applications of artificial neural networks for refrigeration, air-conditioning and heat pump systems—A review. Renew. Sustain. Energy Rev. 16, 1340–1358. doi:10.1016/j.rser.2011.10.015

Monfared, B., Furberg, R., Palm, B., 2014. Magnetic vs. vapor-compression household refrigerators: A preliminary comparative life cycle assessment. Int. J. Refrig. 42, 69–76. doi:10.1016/j.ijrefrig.2014.02.013

Qian, G., Yong, H., 2013. Forecasting the Rural Per Capita Living Consumption Based on Matlab BP Neural Shanghai University of Engineering Science 4, 131–137.

Refaeilzadeh, P., Tang, L., Liu, H., 2009. Cross-Validation, in: LIU, L., ÖZSU, M.T. (Eds.), Encyclopedia of Database Systems. Springer US, Boston, MA, pp. 532–538. doi:10.1007/978-0-387-39940-9_565

Roy, S., Poncet, S., Sorin, M., 2017. Sensitivity analysis and multiobjective optimization of a parallel-plate active magnetic regenerator using a genetic algorithm. Int. J. Refrig. 75, 276–285. doi:10.1016/j.ijrefrig.2017.01.005

Sheela, K.G., Deepa, S.N., 2013. Review on methods to fix number of hidden neurons in neural networks. Math. Probl. Eng. 2013. doi:10.1155/2013/425740

Teyber, R., Trevizoli, P. V, Niknia, I., Christiaanse, T. V, Govindappa, P., Rowe, A., 2016. Experimental performance investigation of an active magnetic regenerator subject to different fluid flow waveforms. Int. J. Refrig. 3, 6–4. doi:10.1016/j.ijrefrig.2016.10.001

Trevizoli, P., Liu, Y., Tura, A., Rowe, A., Barbosa, J., 2014. Experimental assessment of the thermal-hydraulic performance of packed-sphere oscillating-flow regenerators using water. Exp. Therm. Fluid Sci. 57, 324–334. doi:10.1016/j.expthermflusci.2014.06.001

Trevizoli, P. V., Nakashima, A.T., Peixer, G.F., Barbosa, J.R., 2016. Performance evaluation of an active magnetic regenerator for cooling applications - part I: experimental analysis and thermodynamic performance. Int. J. Refrig. doi:10.1016/j.ijrefrig.2016.07.009

Tura, A., Rowe, A., 2014. Concentric Halbach cylinder magnetic refrigerator cost optimization. Int. J. Refrig. 37, 106–116. doi:10.1016/j.ijrefrig.2013.09.005

Tura, A., Rowe, A., 2011. Permanent magnet magnetic refrigerator design and experimental characterization. Int. J. Refrig. 34, 628–639. doi:10.1016/j.ijrefrig.2010.12.009

Tušek, J., Kitanovski, A., Poredoš, A., 2013a. Geometrical optimization of packed-bed and parallel-plate active magnetic regenerators, in: International Journal of Refrigeration. pp. 1456–1464. doi:10.1016/j.ijrefrig.2013.04.001

Tušek, J., Kitanovski, A., Zupan, S., Prebil, I., Poredoš, A., 2013b. A comprehensive experimental analysis of gadolinium active magnetic regenerators. Appl. Therm. Eng. 53, 57–66. doi:10.1016/j.applthermaleng.2013.01.015

Velázquez, D., Estepa, C., Palacios, E., Burriel, R., 2016. A comprehensive study of a versatile magnetic refrigeration demonstrator. Int. J. Refrig. 63, 14–24. doi:10.1016/j.ijrefrig.2015.10.006

Zimm, C., Auringer, J., Boeder, a, Chell, J., Russek, S., Sternberg, a, 2007. Design and initial performance of a magnetic refrigerator with a rotating permanent magnet. Proc. 2^\mathrm{nd} Int. Conf. Magn. Refrig. Room Temp. Portoroz, Slov. 341–347. doi:10.4065/mcp.2010.0817